Wadi Alshatti University Journal of Pure and Applied Sciences

مجلة جامعة وادي الشاطئ للعلوم البحتة والتطبيقية

Volume 4, No. 2, July-December 2026 Online ISSN: 3006-0877 المجلد 4، الاصدار 2، يوليو-ديسمبر 2026

RESEARCH ARTICLE CHEMICAL ENGINEERING

A Hybrid Steady-State Mathematical Model for a Brine-Recycle Multistage Flash Desalination System

Mohamed Elamin Abduljawad[1,*]

[1]Libyan Authority for Scientific Research, Tripoli, Libya

ARTICLE HISTORY
Received 17 April 2026
Revised 08 June 2026
Accepted 30 June 2026
Online 08 July 2026

KEYWORDS
Multistage Flash Desalination;
Brine-Recycle MSF (MSF-BR);
Steady-State Mathematical Modelling;
Section-Wise Modelling;
Iterative Linearization.

ABSTRACT

A steady-state mathematical model for a brine-recycle multistage flash (MSF-BR) desalination system is developed for performance prediction and analysis. The proposed formulation combines the computational simplicity of section-wise steady-state models with selected rigorous thermodynamic features while avoiding the complexity of detailed stage-by-stage formulations. The governing model consists of coupled mass, salt, and energy balance equations combined with heat-transfer relations for the recovery section, rejection section, brine heater, and mixing units. The resulting nonlinear algebraic equations are linearized using a modified tridiagonal model (TDM)-based approach and solved iteratively within a FORTRAN computational framework. The model is validated using published benchmark data for a 5 MGD brine-recycle MSF desalination plant reported by Rosso et al. Predicted temperatures, flow rates, salinities, heat-transfer coefficients, distillate production, and gain output ratio (GOR) show good agreement with the reference results, with deviations generally within acceptable engineering limits. The model also reproduces the effects of steam and seawater temperatures on plant performance. While deviations in distillate production and gain output ratio increase at elevated steam temperatures, the agreement remains satisfactory within the practical operating range of MSF desalination plants. The results demonstrate that the proposed model provides reliable steady-state predictions with moderate computational effort. Owing to its balance between physical realism and numerical simplicity, the model represents a practical tool for simulation, parametric analysis, and preliminary optimization of large-scale MSF desalination systems.

نموذج رياضي هجين عند حالة الاستقرار لمحطة تحلية المياه متعددة المراحل بالتبخير الوميضي مع إعادة تدوير المحلول الملحي

محمد الأمين عبد الجواد[1,*]

الكلمات المفتاحية

التحلية بالتبخير الوميضي متعدد المراحل
إعادة تدوير المحلول الملحي
النمذجة في الحالة المستقرة
النمذجة الرياضية
النمذجة المقطعية
الخطية التكرارية

الملخص

تم تطوير نموذج عند حالة الاستقرار لمحطة تحلية المياه متعددة المراحل بتقنية التبخير الوميضي و إعادة تدوير المحلول الملحي (MSF-BR)، وذلك بهدف التنبؤ بالأداء وتحليله. وقد تمت صياغة النموذج على شكل مجموعة من المعادلات الجبرية غير الخطية المترابطة والمستندة إلى مبادئ حفظ الكتلة والطاقة وانتقال الحرارة. يجمع النموذج بين بساطة نماذج الحالة المستقرة القائمة على التحليل المقطعي وبعض الخصائص الثرموديناميكية التي تشمل اعتماد الخواص الثرموفيزيائية على درجة الحرارة والملوحة، وزيادة درجة الغليان (BPE)، و معامل عدم الاتزان (NEA) ، والانخفاض في درجة الحرارة عبر مزيل الرذاذ (demister) . تم تحويل المعادلات غير الخطية إلى نظام من المعادلات الخطية باستخدام الطريقة المتبعة بالنموذج ثلاثي الأقطار(TDM) ، مما يتيح حله بكفاءة من خلال إجراء تكراري مع تقليل الجهد الحسابي. تم تنفيذ النموذج الرياضي باستخدام بيئة تعتمد على لغة FORTRAN، مع تحقيق التقارب وفق معايير محددة. وقد تم التحقق من صحة النموذج باستخدام بيانات مرجعية منشورة لمحاكاة محطة تحلية MSF-BR بسعة 5 ملايين جالون يوميًا، حيث تمت مقارنة النتائج المتوقعة مع تلك المنشورة من قبل Rosso وآخرين. وقد أظهرت المتغيرات المحسوبة، بما في ذلك توزيعات درجات الحرارة، و إنتاج المياه المحلاة ، وتراكيز الملوحة، ومعاملات انتقال الحرارة، ونسبة وحدات الإنتاج للبخار المستهلك (GOR)، توافقًا جيدًا مع النتائج المرجعية، مع انحرافات ضمن الحدود الهندسية المقبولة، كما نجح النموذج في تمثيل تأثيرات درجات حرارة البخار ومياه البحر على أداء المحطة. وتُظهر النتائج أن النموذج المقترح يوفر تنبؤات موثوقة عند حالة الاستقرار مع جهد حسابي معتدل، مما يجعله أداة عملية لتقييم الأداء، وإجراء الدراسات البارامترية، وتحسين أنظمة تحلية المياه متعددة المراحل واسعة النطاق.

*Corresponding author
https://doi.org/10.63318/waujpasv4i2_10

Introduction

The multistage flash (MSF) process remains one of the most reliable and mature desalination technologies, particularly in regions such as the Middle East and the Mediterranean basin, where freshwater scarcity is severe. Owing to its long operational history, robustness, and ability to operate at very large scales, MSF continues to play an important role in large-scale water production, especially when integrated with dual-purpose power–water plants or implemented in hybrid configurations combined with reverse osmosis (RO). Although MSF once accounted for more than 90% of global thermal desalination capacity, recent assessments indicate that it now represents around 17% of the total installed desalination capacity worldwide [1,2]. Despite this decline, MSF remains one of the dominant thermal desalination technologies and continues to be strategically important for countries that rely heavily on large-scale seawater desalination. In Libya, where MSF has historically been the predominant desalination technology, the country's total installed desalination capacity is estimated at approximately 600,000 m^3/day [3].

Recent studies have also explored the integration of renewable thermal energy technologies with desalination systems to improve energy efficiency and reduce environmental impacts. Examples include solar thermal-powered desalination systems and the use of Linear Fresnel Collectors (LFCs) as sustainable heat sources for thermal desalination processes [4,5]. Regardless of the heat source employed, however, accurate mathematical models remain essential for the simulation, design, optimization, performance evaluation, and further development of MSF desalination systems.

Over the past decades, several steady-state models have been developed to describe MSF behaviour under different design and operating conditions. These models are generally classified into two categories. Simplified models rely on idealized assumptions such as linear temperature profiles, constant heat-transfer coefficients, and fixed brine properties. These assumptions simplify the mass and energy balance equations and make the models suitable for preliminary design and performance estimation [6–9]. Such models require relatively low computational effort and are widely used for initial analysis of MSF plants. Rigorous models, on the other hand, provide detailed stage-by-stage representations of thermodynamic and heat-transfer behaviour, although they require greater mathematical complexity and computational effort. Representative examples of both modelling approaches are widely reported in the literature [10–15].

Soliman [7] developed one of the earliest simplified steady-state models for MSF desalination plants, intended for rapid performance estimation and preliminary optimization. Although simplified, Soliman's formulation retains the essential characteristics of more complex models while substantially reducing computational effort. The model is based on several simplifying assumptions, including linear temperature profiles, constant overall heat-transfer coefficients and thermophysical properties within each section, constant latent heat of vaporization, and equal distillate production in all stages. These assumptions permit section-wise analysis rather than detailed stage-by-stage calculations, resulting in a model that is straightforward to implement and suitable for rapid performance estimation. However, the assumption of constant thermophysical properties limits the model accuracy, particularly in high-temperature regions where seawater properties vary significantly with temperature and salinity.

In contrast, Helal et al. [10] proposed a rigorous stage-by-stage tridiagonal model (TDM) capable of representing the detailed thermodynamic and heat-transfer behavior of MSF plants under realistic operating conditions. Their formulation applies a systematic linearization procedure to the strongly nonlinear governing equations, producing a matrix system that can be solved iteratively for stage temperatures and flow rates. Although the TDM model improves predictive accuracy, the large number of equations and variables increases the mathematical complexity and computational effort required for implementation and analysis.

Recent studies demonstrate that both simplified section-wise models and rigorous stage-wise formulations continue to be actively applied in MSF simulation, optimization, and performance analysis. Abduljawad and Ezzeghni [16] employed simplified steady-state formulations for optimization of the Tajoura MSF plant, while Abujazyah [17] developed a linearized stage-wise model based on a tridiagonal matrix formulation for an operating Libyan MSF plant. Hassanean et al. [18] developed a steady-state simulation model for an MSF brine-circulation desalination plant in which the nonlinear governing equations were linearized and arranged in tridiagonal matrix form to predict stage temperatures, flow rates, and plant productivity. Rigorous steady-state frameworks have also been implemented in advanced simulation environments such as gPROMS for performance prediction and fouling analysis [19,20]. In addition, Al-Fulaij [21] developed steady-state and dynamic models for MSF-OT and MSF-BR systems using formulations derived from Helal's methodology. These studies confirm that both Soliman-type simplified models and Helal-type rigorous formulations remain relevant for contemporary MSF analysis, particularly for simulation, optimization, and operational studies.

However, despite these developments, there remains a need for computationally efficient models that incorporate improved thermophysical-property representation without the full complexity of detailed stage-wise formulations.

The present work aims to bridge the gap between simplified section-wise models and rigorous stage-wise formulations. The proposed model retains the computational simplicity of the section-wise approach originally introduced by Soliman while incorporating selected rigorous thermodynamic features inspired by the TDM methodology of Helal et al.

In particular, the model relaxes the assumptions of constant specific heat capacity and constant latent heat of vaporization by accounting for the variation of thermophysical properties with temperature and salinity. In addition, boiling-point elevation (BPE), non-equilibrium allowance (NEA), and demister temperature losses are incorporated explicitly into the formulation. To preserve computational efficiency, the assumptions of linear temperature profiles and section-wise averaged heat-transfer coefficients are retained, allowing the governing equations to be formulated on a section basis rather than a stage basis. The resulting nonlinear equations are subsequently linearized using a modified TDM-based procedure adapted for the reduced section-wise formulation.

Consequently, the proposed model provides a practical compromise between physical realism, predictive capability, and computational simplicity, making it suitable for steady-state simulation, parametric analysis, and preliminary optimization of MSF-BR desalination systems.

To the authors' knowledge, the combination of a reduced section-wise MSF formulation, temperature-dependent thermophysical properties, and a TDM-inspired linearization framework within a single steady-state model has not been previously reported. The detailed derivation of the governing equations, linearization procedure, and numerical solution method are presented in the following sections.

Process description

A schematic diagram of the brine-recycle multistage flash (MSF-BR) desalination plant considered in the present study is shown in Fig. 1. The process consists of three principal sections: the heat recovery section, the heat rejection section, and the brine heater. The plant configuration incorporates brine recycle circulation together with cooling seawater intake and reject seawater discharge.

Cooling seawater enters the heat rejection section at temperature T_{F_4} and flow rate W_T. As it flows through the condenser tubes of the rejection stages, it absorbs heat released by the condensing flash vapor and leaves the rejection section at temperature T_{F_3}. The outlet stream is then divided into two parts: a reject seawater stream W_C, discharged back to the sea, and a make-up seawater stream F, which is directed to the mixing point.

The make-up seawater stream mixes with the recycle brine stream R returning from the final stage of the plant. The combined stream, denoted by W, enters the heat recovery section at temperature T_{F_2}. As the stream flows through the condenser tubes of the recovery stages, it is progressively heated by condensation of flash vapor generated from the flashing brine flowing through the stages. Consequently, the cooling brine temperature increases gradually along the recovery section and leaves at temperature T_{F_1}.

The heated brine stream then enters the brine heater, where external steam at saturation temperature T_S supplies the thermal energy required to raise the brine temperature to the top brine temperature T_{B_0} . The heated brine subsequently enters the first flashing stage, where the pressure reduction causes partial flashing of the brine and generation of vapor.

The generated vapor passes through demisters to remove entrained brine droplets before condensing on the outer surfaces of the condenser tubes, thereby producing distillate. The remaining brine flows successively through stages operating at progressively lower pressures and temperatures, generating additional flash vapor in each stage. The condensed vapor from all stages is collected as the distillate product stream.

The concentrated brine leaving the final stage of the rejection section is divided into two streams: the blowdown stream B_D, which is discharged from the plant to control salinity, and the recycle brine stream R, which returns to the mixer and combines with the incoming make-up seawater. The process therefore operates as a closed brine-recycle system in which thermal energy recovery within the recovery section significantly reduces steam consumption in the brine heater.

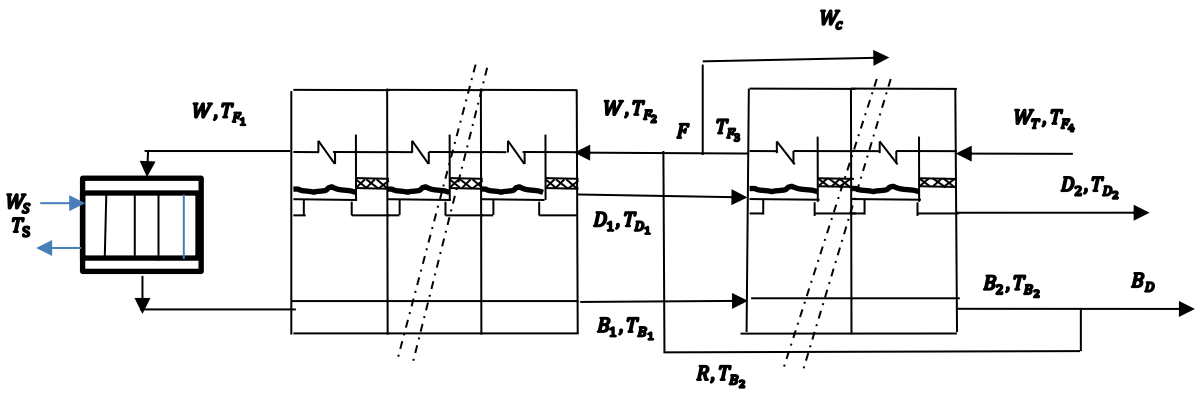

Figure 1: Schematic diagram of a brine-recycle multistage flash desalination process

Mathematical Model

A steady-state mathematical model of the MSF brine-recycle (MSF-BR) desalination plant shown schematically in Fig. 1 is developed in this section. To simplify the analysis while preserving the essential physics of the process, the following assumptions are adopted:

- Linear temperature profiles for all streams flowing within the plant.
- Constant heat-transfer coefficient and heat-transfer area within each section.
- Thermophysical properties of seawater—such as specific heat capacity, latent heat of vaporization, and boiling-point elevation—are treated as functions of temperature and salinity.
- The distillate is salt-free, and each stage produces an equal distillate flow rate.
- Heat losses to the surroundings are negligible.

The first three assumptions constitute the core of the present section-wise modeling approach and are justified as follows:

The assumption of linear temperature profiles within each section, originally introduced by Soliman, is supported by both practical observations and detailed stage-wise simulations, which consistently show a quasi-linear variation of temperature with stage number. This behavior arises from the uniformity of stage geometry (equal tube length, diameter, and heat-transfer area) and the nearly uniform temperature driving force across stages. The gradual temperature rise of the cooling brine inside the tubes is approximately balanced by the temperature decrease of the flashing brine along successive stages, resulting in an overall linear temperature distribution.

Closely related to this, the assumption of a constant heat-transfer coefficient within each section enables the aggregation of stage-wise heat-transfer relations into a single section-wise equation. This simplification, also adopted in classical models such as that of Soliman, is justified by the relatively small variation in operating conditions between

stages within the same section. In the present model, this assumption is partially relaxed by evaluating the heat-transfer coefficient at representative mid-section conditions, thereby improving physical realism while preserving computational simplicity.

The third assumption introduces a key refinement over earlier simplified models by accounting for the dependence of thermophysical properties on temperature and salinity. In contrast to classical approaches that assume constant specific heat capacity and latent heat of vaporization throughout the plant, the present formulation evaluates these properties as functions of local temperature and salinity conditions. This enhancement improves the accuracy of predicted heat duties and temperature profiles, particularly in high-temperature regions such as the brine heater.

The remaining assumptions—namely, salt-free distillate production with equal stage-wise yield, and negligible heat losses—are standard in MSF modelling and are widely accepted due to their minimal impact on overall plant performance predictions.

The governing equations are formulated by applying overall mass, salt, and energy balances to the recovery, rejection, and brine-heater sections. The overall heat-transfer rate between the flashing vapor and the cooling brine in each section is evaluated by first applying the heat-transfer equation at the last stage of the section, and then multiplying the resulting duty by the number of stages in that section.

The temperature dependencies of the boiling-point elevation (BPE), non-equilibrium allowance (NEA), and the temperature drop across the demister at the last stage of each section are incorporated to determine the temperature differences between the flashing brine and the condensed vapor leaving the section (T_{D_1} and T_{D_2}).

Governing Equations

Mass and salt balances

Recovery section

The overall mass balance

$$W = B_1 + D_1 \quad (1)$$

The corresponding salt balance

$$W C_{B_0} = B_1 C_{B_1} \quad (2)$$

Rejection section

The total mass balance is:

$$B_1 + D_1 = B_2 + D_2 \quad (3)$$

The salt balance is:

$$B_1 C_{B_1} = B_2 C_{B_2} \quad (4)$$

Energy balances

Recovery section

The overall energy balance is expressed as:

$$W\ S_R\left(T_{F_1} - T_{F_2}\right) = W\ S_{B_0}\left(T_{B_0} - T^*\right) - D_1\ S_{D_1}\left(T_{D_1} - T^*\right) - B_1\ S_{B_1}\left(T_{B_1} - T^*\right) \quad (5)$$

Recovery condenser energy balance

$$W\ S_R\left(T_{F_1} - T_{F_2}\right) = \lambda_R D_1 \quad (6)$$

Rejection section

$$W_T\ S_J\left(T_{F_3} - T_{F_4}\right) = B_1\ S_{B_1}\left(T_{B_1} - T^*\right) + D_1\ S_{D_1}\left(T_{D_1} - T^*\right) - D_2\ S_{D_2}\left(T_{D_2} - T^*\right) - B_2\ S_{B_2}\left(T_{B_2} - T^*\right) \quad (7)$$

Rejection condenser energy balance

$$W_T\ S_J\left(T_{F_3} - T_{F_4}\right) = \lambda_J D_2 \quad (8)$$

where S_i denote the effective specific heat capacities of the corresponding streams, evaluated at the average section temperatures.

Heat transfer relations

Recovery Section

$$W\ S_R\left(T_{F_1} - T_{F_2}\right) = N_R\ U_R\ A_R\ \Delta T_{lm,R} \quad (9)$$

Where the logarithmic mean temperature difference is:

$$\Delta T_{lm,R} = \frac{(T_{F_1} - T_{F_2})/N_R}{ln\left(\frac{T_{D_1} - T_{F_2}}{T_{D_1} - \left(T_{F_2} + \frac{T_{F_1} - T_{F_2}}{N_R}\right)}\right)}$$

The logarithmic mean temperature difference in Eq. (9) is derived based on the assumption of a linear temperature profile along the recovery section, which implies equal temperature drops across all recovery stages. Accordingly, the temperature drop per stage is given by

$$\left(T_{F_1} - T_{F_2}\right)/N_R$$

where N_R is the number of recovery stages.

The lower temperature-difference limit corresponds to the inlet temperature of the last recovery stage, T_{F_2}, while the upper limit is obtained from the linear-profile assumption as

$$T_{F_2} + \frac{T_{F_1} - T_{F_2}}{N_R}$$

Hence, the temperature difference at the last stage becomes

$$\left(T_{F_2} + \frac{T_{F_1} - T_{F_2}}{N_R}\right) - T_{F_2} = \frac{T_{F_1} - T_{F_2}}{N_R}$$

which forms the numerator of the logarithmic mean temperature difference expression. The denominator is obtained from the ratio of the inlet and outlet stage temperature differences associated with the condensation temperatures outside the tubes.

Rejection section

$$W_T\ S_J\left(T_{F_3} - T_{F_4}\right) = N_J\ U_J\ A_J\ \Delta T_{lm,J} \quad (10)$$

where:

$$\Delta T_{lm,J} = \frac{(T_{F_3} - T_{F_4})/N_J}{ln\left(\frac{T_{D_2} - T_{F_4}}{T_{D_2} - \left(T_{F_4} + \frac{T_{F_3} - T_{F_4}}{NJ}\right)}\right)}$$

Brine heater

$$W\ S_H\left(T_{B_0} - T_{F_1}\right) = U_H\ A_H\ \frac{(T_{B_0} - T_{F_1})}{ln\left(\frac{T_S - T_{F_1}}{T_S - T_{B_0}}\right)} \quad (11)$$

Mixing and splitting relations

Mass balance on blowdown splitter

$$B_D = B_2 - R \quad (12)$$

Mass balance on reject seawater splitter

$$F = W_T - W_C \quad (13)$$

Mixer mass balance

$$W = F + R \quad (14)$$

Mixer salt balance

$$W C_{B_0} = R\ C_{B_2} + F\ C_F \quad (15)$$

Mixer energy balance

$$W S_W\left(T_{F_2} - T^*\right) = R S_{RY}\left(T_{B_2} - T^*\right) + F\ S_F\left(T_{F_3} - T^*\right) \quad (16)$$

Temperature Relations

The brine and distillate temperatures are related by:

$$T_{B_1} = T_{D_1} + BPE_1 + NEA_1 + \Delta_1 \quad (17)$$

$$T_{B_2} = T_{D_2} + BPE_2 + NEA_2 + \Delta_2 \quad (18)$$

where

BPE_i = Boiling point elevation

NEA_i = non-equilibrium allowance

Δ_i = Temperature loss across the demister

The process flow diagram shown in fig.1 provides the physical basis for the formulation of the governing equations. Each stream and control volume identified in the figure corresponds directly to the mass, salt, and energy balance equations presented in this section, in particular, the recovery

and rejection sections illustrated in Fig. 1 form the basis for Eqs. (1)–(8), while the brine heater and mixing units correspond to Eqs. (11) and (16), respectively. This direct correspondence ensures consistency between the physical process representation and the mathematical formulation of the MSF-BR system.

Model linearization

The governing equations of the MSF-BR model are inherently nonlinear due to the strong coupling between temperatures, flow rates, and thermophysical properties. These nonlinearities arise primarily from the temperature dependence of physical properties and the logarithmic nature of the heat-transfer relations. To obtain a computationally efficient solution, the present study adopts the linearization approach proposed by Helal et al. in their TDM (Tri-Diagonal Model) formulation.

In this approach, the nonlinear system is linearized by selecting a set of primary unknown variables. All remaining variables, including thermophysical properties, flow rates, and intermediate temperatures, are incorporated into coefficients evaluated using values from the previous iteration. These coefficients are therefore treated as constants within each iteration step and constitute the coefficients of the linearized equations. The resulting linear system is solved, and the updated temperature values are subsequently used to recompute the coefficients. This iterative procedure continues until convergence is achieved.

This approach significantly simplifies the numerical solution while preserving the essential nonlinear characteristics of the system through iterative coefficient updates.

Selection of Linearization Variables

For the brine-recycle MSF system, the following temperatures are selected as the primary unknowns:

T_{B_0} , T_{F_1}, T_{F_2} , T_{F_3}.

These variables were selected because they represent the key thermal states of the heat transfer processes in the subsequent sections of the plant, as well as the mixing point, thereby interconnecting the linearized equations, where each equation combines at least two or three successive primary variables of the linearized system. Furthermore, the other plant temperature profiles (brine and distillate temperatures) are related to these primary temperatures through heat transfer and temperature-loss relations; hence, once these primary temperatures are determined, all other system temperatures can be obtained.

The remaining variables, including flow rates, thermophysical properties, are expressed in terms of these selected variables and the related plant temperatures, which are incorporated into lumped coefficients evaluated during each iteration.

Linear System Formulation

The following governing relations are selected as the basis of the linearized system:

- Overall energy balance on the recovery section (Eq. 5)
- Overall energy balance on the rejection section (Eq. 7)
- Heat-transfer equation in the brine heater (Eq. 11)
- Energy balance on the mixer (Eq. 16)

After linearization, these relations yield a system of four linear algebraic equations of the general form:

$$C_{1_j}T_{B_0} + C_{2_j}T_{F_1} + C_{3_j}T_{F_2} + C_{4_j}T_{F_3} = C_{5_j} \quad (19)$$

where the coefficients C_{i_j} are functions of flow rates and thermophysical properties evaluated from the previous iteration and are therefore treated as constants within each iteration step.

Once the coefficients are fixed, the resulting linear system is solved simultaneously to obtain updated values of the selected variables. All remaining model variables are then determined using the corresponding governing relations. The procedure is repeated until convergence is achieved. The iterative solution is considered converged when the sum of squared differences between successive brine-temperature iterations becomes less than10^{-9}.

The selection of a section-wise formulation, rather than a detailed stage-by-stage representation, is motivated by the need to reduce computational complexity while maintaining sufficient physical accuracy. In this approach, the thermal behavior of each section is represented by averaged properties and lumped parameters, which significantly reduces the number of governing equations. This simplification is particularly advantageous for iterative solution procedures and parametric studies, while still preserving the dominant heat- and mass-transfer characteristics of the MSF process.

Development of the Linearized Model

The linearization procedure starts by rearranging the heat-transfer relations for the recovery and rejection sections, Eqs. (9) and (10), in order to express the distillate temperatures T_{D_1} and T_{D_2} as linear functions of the selected temperature variables T_{F_1}, T_{F_2}, T_{F_3} and T_{F_4}.This yields

$$T_{D_1} = \frac{T_{F_1}}{N_R\ \alpha_R} + \frac{N_R\ \alpha_R - 1}{N_R\ \alpha_R} T_{F_2} \quad (20)$$

$$T_{D_2} = \frac{T_{F_3}}{N_J\ \alpha_J} + \frac{N_J\ \alpha_J - 1}{N_J\ \alpha_J} T_{F_4} \quad (21)$$

Where α_R and α_J are evaluated from condition of previous iteration and are defined as follows:

$$\alpha_R = 1 - EXP\left(\frac{-U_R\ A_R}{W\ S_R}\right) \quad (22)$$

$$\alpha_J = 1 - EXP\left(\frac{-U_J\ A_J}{W_T\ S_J}\right) \quad (23)$$

Based on the latest available numerical values, the boiling-point elevation, non-equilibrium allowance, and demister temperature loss are treated as constants during each iteration. Thus, Eqs. (17) and (18) The brine and Distillate temperatures relations become:

$$T_{B_1} = T_{D_1} + Z_1 \quad (24)$$

$$T_{B_2} = T_{D_2} + Z_2 \quad (25)$$

Where

$$Z_1 = BPE_1 + NEA_1 + \Delta_1 \quad (26)$$

$$Z_2 = BPE_2 + NEA_2 + \Delta_2 \quad (27)$$

Linearized Energy Balance: Recovery Section

Rearranging the overall energy balance for the recovery section, Eq. (5), gives

$$T_{F_1} - T_{F_2} = a_{2_R}T_{B_0} - a_{3_R}T_{D_1} - a_{4_R}T_{B_1} + a_{5_R} \quad (28)$$

Where

$$a_{2_R} = \frac{W\ S_{B_0}}{W\ S_R} \qquad a_{3_R} = \frac{D_1\ S_{D_1}}{W\ S_R}$$

$$a_{4_R} = \frac{B_1\ S_{B_1}}{W\ S_R} \qquad a_{5_R} = T^*\left(a_{4_R} + a_{3_R} - a_{2_R}\right)$$

Substituting Eq. (24) into Eq. (28) yields:

$$T_{F_1} - T_{F_2} = b_{1_R}T_{B_0} + b_{2_R}T_{D_1} + b_{3_R} \quad (29)$$

With

$$b_{1_R} = a_{2_R}, \quad b_{2_R} = -\left(a_{3_R} + a_{4_R}\right), \quad b_{3_R} = a_{5_R} - a_{4_R}Z_1.$$

Eliminating T_{D_1} using Eq. (20), the recovery-section energy balance becomes:

$$C_{1_R}T_{B_0} + C_{2_R}T_{F_1} + C_{3_R}T_{F_2} = C_{5_R} \quad (30)$$

Where

$$C_{1_R} = b_{1_R}\ , \qquad C_{2_R} = \left(\frac{b_{2_R}}{N_R\alpha_R} - 1\right),$$

$$C_{3R} = \left(1 + b_{2R} - \frac{b_{2R}}{N_R \alpha_R}\right), \qquad C_{5R} = -b_{3R}$$

Linearized Energy Balance: Rejection Section

Similarly, rearranging the overall energy balance for the rejection section (Eq. 6) yields:

$$T_{F_3} - T_{F_4} = a_{1_J} T_{D_1} + a_{2_J} T_{B_1} - a_{3_J} T_{D_2} - a_{4_J} T_{B_2} + a_{5_J} \quad (31)$$

Where

$$a_{1_J} = \frac{D_1 S_{D_1}}{W_T S_J} \qquad a_{2_J} = \frac{B_1 S_{B_1}}{W_T S_J}$$

$$a_{3_J} = \frac{D_2 S_{D_2}}{W_T S_J} \qquad a_{4_J} = \frac{B_2 S_{B_2}}{W_T S_J}$$

$$a_{5_J} = T^* \left(a_{3_J} + a_{4_J} - a_{1_J} - a_{2_J}\right)$$

Substituting Eqs. (24) and (25) gives

$$T_{F_3} - T_{F_4} = b_{1_J} T_{D_1} + b_{2_J} T_{D_2} + b_{3_J} \quad (32)$$

With

$$b_{1_J} = a_{1_J} + a_{2_J}, \qquad b_{2_J} = -\left(a_{3_J} + a_{4_J}\right),$$

$$b_{3_J} = a_{5_J} + a_{2_J} Z_1 - a_{4_J} Z_2.$$

Eliminating T_{D_1} and T_{D_2} using Eqs. (20) – (21), the rejection-section energy balance becomes:

$$C_{2_J} T_{F_1} + C_{3_J} T_{F_2} + C_{4_J} T_{F_3} = C_{5_J} \quad (33)$$

Where

$$C_{2_J} = \frac{b_{1_J}}{N_R \alpha_R}, \qquad C_{3_J} = \left(b_{1_J} - \frac{b_{1_J}}{N_R \alpha_R}\right),$$

$$C_{4_J} = \left(\frac{b_{2_J}}{N_J \alpha_J} - 1\right),$$

$$C_{5_J} = \left(\frac{b_{2_J}}{N_J \alpha_J} - b_{2_J} - 1\right) T_{F_4} - b_{3_J}.$$

Linearized Energy Balance: Brine-Heater

The linear form of the brine heater equation is obtained by rearranging Eq. (11) as:

$$C_{1_H} T_{B_0} + C_{2_H} T_{F_1} = C_{5_H} \quad (34)$$

with

$$C_{1_H} = 1, \qquad C_{2_H} = (\alpha_H - 1), \qquad C_{5_H} = \alpha_H T_{S.}$$

Where α_H is evaluated from condition of previous iteration and is defined as follows:

$$\alpha_H = 1 - EXP\left(\frac{-U_H A_H}{W S_H}\right) \quad (35)$$

Linearized Energy Balance: Mixer

Starting from the energy balance on the mixer (Eq. 16), and substituting Eqs. (25) and (21) to eliminate T_{B_2} and T_{D_2}, the mixer energy balance is linearized as:

$$C_{3_M} T_{F_2} + C_{4_M} T_{F_3} = C_{5M} \quad (36)$$

where

$$C_{3_M} = W S_W, \qquad C_{4_M} = -\left(F S_F + \frac{R S_{Ry}}{N_J \alpha_J}\right),$$

$$C_{5_M} = b_m + \frac{R S_{Ry}\left(N_J \alpha_J - 1\right)}{N_J \alpha_J} T_{F_4},$$

$$b_m = a_m + R S_{Ry} Z_{2,}$$

$$a_m = \left(W S_W - R S_{Ry} - F S_F\right) T^*.$$

Overall Matrix Form

The complete linearized system is expressed in matrix form:

$$\begin{bmatrix} 1 & C_{2H} & 0 & 0 \\ C_{1_R} & C_{2_R} & C_{3_R} & 0 \\ 0 & 0 & C_{3_M} & C_{4_M} \\ 0 & C_{2_J} & C_{3_J} & C_{4_J} \end{bmatrix} \times \begin{bmatrix} T_{B_0} \\ T_{F_1} \\ T_{F_2} \\ T_{F_3} \end{bmatrix} = \begin{bmatrix} C_{5_H} \\ C_{5_R} \\ C_{5_M} \\ C_{5_J} \end{bmatrix} \quad (37)$$

Numerical solution procedure

The numerical solution procedure adopted in this study is summarized in Algorithm 1. The required plant design and operating parameters $(W_T, R, W_C, T_{F_4}, T_S, C_F)$ are first specified. Initial estimates are assigned for the cooling brine, distillate and flashing-brine temperatures together with the corresponding brine concentrations.

The overall mass balances on the reject seawater splitter and mixer are then solved to determine the main flow rates. The mixer salt balance is subsequently solved to determine the cooling-brine salinity entering the last recovery stage.

Section-wise mass balances are subsequently applied to calculate distillate and brine flow rates. Heat-transfer parameters and linearization coefficients are evaluated, and the corresponding linear algebraic matrix coefficients are assembled. The resulting linear algebraic system is solved simultaneously to obtain updated values of the cooling-brine and top-brine temperatures. The distillate and brine temperatures are then recalculated.

The solution procedure is repeated iteratively until convergence of the brine temperatures is achieved. Upon convergence, the final temperature profiles, flow rates, and performance parameters are obtained.

Algorithm 1. Numerical solution procedure for the MSF-BR desalination plant

Input data

Read plant and feed parameters: $W_T, R, W_C, T_{F_4}, T_S, C_F$

Initialization

Assume initial values for

$T_{B_0}, T_{F_1}, T_{F_2}, T_{F_3}, T_{B_1}, T_{B_2}, T_{D_1}, T_{D_2}, C_{B_0}$.

Step 1: Overall balances

Apply (13–14) to evaluate F, W.

Step 2: Mixer salt balance

Apply Eq. (15) to update the flashing brine salinity entering first recovery stage C_{B_0}.

Step 3: Section mass balances

Solve Eqs. (6) and (8) to compute D_1, D_2 and apply Eqs. (1)–(4) to compute B_1, B_2 and corresponding concentrations C_{B_1}, C_{B_2}.

Step 4: Heat-transfer evaluation

Evaluate Z_1, Z_2, U_R, U_J and U_H, then calculate α_R, α_J and α_H.

Step 5: Coefficient evaluation

Compute coefficients: a_{i_R}, a_{i_J}, a_M, b_{i_R}, b_{i_J}, b_M.

Step 6: Matrix assembly

Form the linear system coefficients $C_{1_R}, C_{2_R}, C_{3_R}, C_{5_R}$, $C_{2_J}, C_{3_J}, C_{4_J}, C_{5_J}$, $C_{1_H}, C_{2_H}, C_{5_H}$, C_{3_M}, C_{4_M}, C_{5_M}.

Step 7: Matrix solution

Solve the linear system Eq. (37) to obtain updated values of: $T_{B_0}, T_{F_1}, T_{F_2}, T_{F_3}$.

Step 8: Temperature update

Calculate T_{D_1} and T_{D_2} using Eqs. (20)-(21).

Step 9: Brine-temperatures update

Extract new values of T_{B_1}, T_{B_2} using Eqs. (24)-(25).

Step 10: Convergence check If:

$$\sum_{j=1}^{2} \left(T_{B_j}^{(new)} - T_{B_j}^{old}\right)^2 \leq 10^{-9}$$

The solution is considered converged when the cumulative squared temperature residual becomes less than 10^{-9}; otherwise, return to Step 2..

Step 11: Output results

Report all temperatures, flow rates, salinities, and performance indicators.

The numerical procedure was found to be numerically stable and converged within a few iterations for all operating conditions investigated. The reduced section-wise formulation significantly decreases the computational effort compared with detailed stage-wise models.

Model Application and Validation

In the present work, the developed steady-state model is applied to evaluate the performance of a brine-recycle multistage flash (MSF-BR) desalination system. The specified operating variables include the recycle brine flow rate R, the seawater intake flow rate W_T, the rejected cooling seawater flow rate W_C, and the steam saturation temperature T_S, which together define the operating condition of the MSF-BR plant.

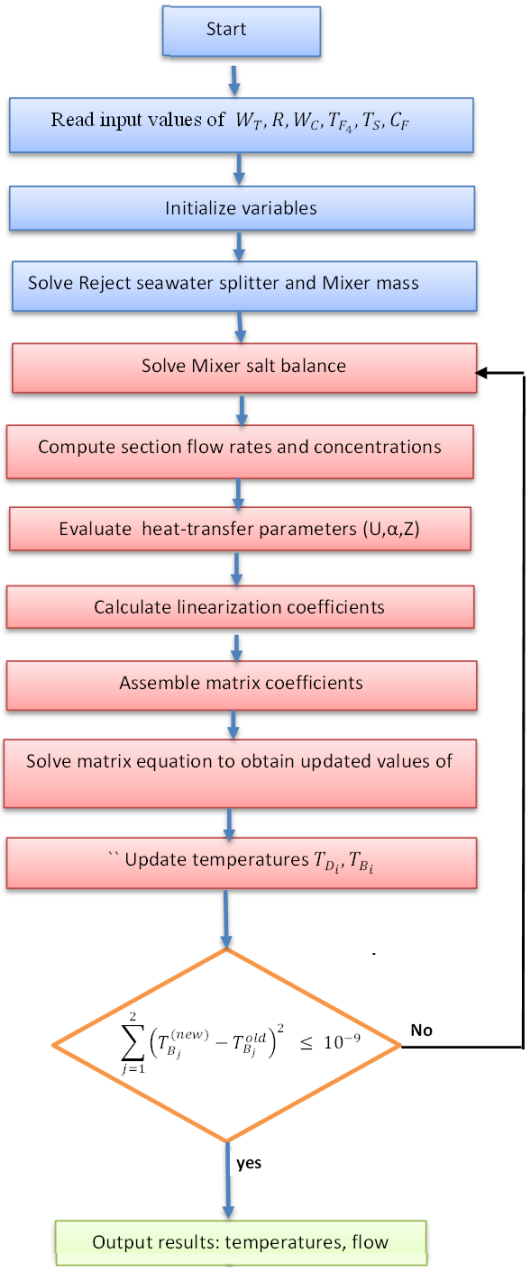

Figure 2: Flowchart of the numerical solution procedure for the steady-state MSF-BR model

Based on these inputs, the model computes the flow rates, temperatures, and salinities of all streams throughout the recovery section, rejection section, and brine heater. Accordingly, key performance indicators such as distillate production rate, specific heat consumption, and gain output ratio (GOR) are evaluated.

The mathematical model was implemented in a FORTRAN program. The numerical solution is obtained through an iterative procedure in which the linearized governing equations are solved repeatedly, and the thermophysical properties are updated at each iteration step. Convergence is achieved when the prescribed tolerance is satisfied. The overall solution algorithm is illustrated in Fig. 2, where mass and energy balances, heat-transfer relations, and property correlations are solved in a coupled manner.

Thermophysical properties of seawater and brine are evaluated using the correlations provided in Appendix A.

Model Validation

The proposed steady-state model was validated using the brine-recycle cross-tube multi-stage flash (MSF) desalination plant reported by Rosso et al. [16], which was originally based on the benchmark configuration introduced by Helal et al. [12].

The reference plant has a nominal production capacity of 5 MGD and consists of 16 stages, including 13 stages in the heat-recovery section and 3 stages in the heat-rejection section. Owing to the availability of detailed operating and design data, this configuration has been widely adopted in the literature as a benchmark for validating MSF performance models.

The operating conditions, heat-transfer areas, tube geometries, fouling factors, and seawater properties used in the present validation are summarized in Table 1. All parameters were taken directly from the published reference data and were applied without adjustment to ensure a consistent and unbiased basis for comparison.

Table 1. Plant design and operational data

Parameter	Value	Unit
Specified operating variables		
Make-up seawater flow rate, W_T	11.3×10^6	kg·h⁻¹
Reject cooling seawater flow rate, W_C	5.62×10^6	kg·h⁻¹
Brine recycle flow rate, R	6.35×10^6	kg·h⁻¹
Steam saturation temperature, T_S	96.6	°C
Seawater inlet temperature	35	°C
Seawater salinity	5.60	wt.%
Heat-transfer areas		
Recovery section (per stage)	3995	m²
Rejection section (per stage)	3530	m²
Brine heater	3530	m²
Tube characteristics		
Heat-recovery section tube length	12.2	m
Heat-rejection section tube length	10.7	m
Brine heater tube length	12.2	m
Number of tubes (each section)	4300	–
Tube material (recovery)	Cu–Ni 90–10	–
Tube material (rejection)	Titanium	–
Tube material (brine heater)	Cu–Ni 70–30	–
Fouling factors		
Recovery section	1.4×10^{-4}	h·m²·K·kcal⁻¹
Rejection section	2.33×10^{-5}	h·m²·K·kcal⁻¹
Brine heater	1.86×10^{-4}	h·m²·K·kcal⁻¹

Flow Rates and Salinity Validation

A comparison between the predicted flow rates and salinities and the reference results of Rosso et al. (1997) is presented in Table 2. The predicted brine flow rates at the outlets of the recovery and rejection sections show very close agreement with the reference values, with deviations not exceeding 0.4%. Similarly, the predicted distillate production rates differ by approximately 3.5–4.2%.

These deviations are within the range commonly reported for steady-state MSF simulations and may be attributed to

differences in thermophysical-property correlations, heat-transfer representations, and fouling-factor evaluation between the present model and the reference formulation.

Table 2: Comparison of predicted and reference flow rates and salinities

Variable	Present model	Rosso et al. (1997)	Deviation (%)
$W\ (kg \cdot h^{-1})$.	1.2030×10^7	1.203×10^7	0.00
$B_1\ (kg \cdot h^{-1})$.	1.1221×10^7	1.125×10^7	−0.26
$B_2\ (kg \cdot h^{-1})$.	1.1056×10^7	1.110×10^7	−0.39
$D_1\ (kg \cdot h^{-1})$.	8.089×10^5	7.780×10^5	+3.96
$D_2\ (kg \cdot h^{-1})$.	9.737×10^5	9.341×10^5	+4.23
C_{B_0} %wt	*6.211*	*6.319*	*−1.70*
C_{B_1} %wt	*6.695*	*6.727*	*+0.48*
C_{B_2} %wt	*6.758*	*6.832*	+1.08

Temperature Validation

Table 3 presents the comparison of predicted temperatures with reference data. Excellent agreement is observed across all sections. Inlet brine temperature to the brine heater and the top brine temperature are reproduced with deviations below 0.4%, indicating that the thermal behavior in high-temperature regions is accurately represented. Outlet temperatures of the recovery and rejection sections also show deviations below 0.2%, demonstrating reliable prediction of axial temperature profiles under steady-state conditions.

Table 3: Comparison of predicted and reference temperatures

Variable	Present model	Rosso et al. (1997)	Deviation (%)
$T_{F_1}(°C)$	*83.66*	*83.33*	+0.39
T_{F_2}°C .	*42.87*	*42.91*	−0.09
$T_{F_3}(°C)$	*43.90*	*43.97*	−0.16
$T_{B_0}(°C)$	*89.99*	*89.74*	+0.28
$T_{B_1}(°C)$	*50.23*	*50.33*	−0.20
$T_{B_2}(°C)$	*41.93*	*41.97*	−0.10
$T_{D_1}(°C)$	*48.65*	*48.73*	−0.16
$T_{D_2}(°C)$	*40.00*	*40.07*	−0.18

Heat-Transfer Coefficients and Performance Indicators

Table 4 compares the predicted average heat-transfer coefficients and overall performance indicators with the reference data. Predicted heat-transfer coefficients in the recovery, rejection sections, and brine heater show good agreement, with deviations generally below 6%. The steam flow rate is slightly lower, while the gain output ratio (GOR) is slightly higher than the reference. These differences reflect small variations in distillate production and heat-transfer calculations, particularly in the rejection section, but remain within acceptable engineering accuracy.

The overall agreement between the present predictions and the benchmark data demonstrates that the proposed section-wise formulation is capable of reproducing the principal thermal and hydraulic characteristics of MSF-BR desalination systems with satisfactory engineering accuracy.

Effect of Operating Temperatures and Model Validation

Figures 3–8 present the effect of heating steam temperature and seawater inlet temperature on key performance parameters of the MSF-BR desalination system. In all cases, the predictions of the present model are plotted together with the reference results reported by Rosso et al., allowing direct visual validation of model performance under identical operating conditions.

Table 4: Comparison of heat-transfer coefficients and performance indicators

Parameter	Present model	Rosso et al. (1997)	Deviation (%)
U_R (kcal·h⁻¹·m⁻²·°C⁻¹)	2218.4	2231.7	−0.60
U_J (kcal·h⁻¹·m⁻²·°C⁻¹)	2731.7	2905.9	−5.99
U_H (kcal·h⁻¹·m⁻²·°C⁻¹)	2075.9	2040.9	+1.73
Steam flow rate (kg·h⁻¹)	133164.9	134898.1	−1.28
Gain output ratio (GOR)	7.31	6.92	+5.63

Effect of heating steam temperature

Figure 3 illustrates the variation of the top brine temperature (TBT) and brine blowdown temperature (BBT) with increasing steam temperature. Both temperatures increase with steam temperature due to the higher thermal energy supplied in the brine heater. The predicted curves closely follow the reference data, reproducing the stronger sensitivity of TBT to steam temperature, while BBT exhibits a comparatively weaker response.

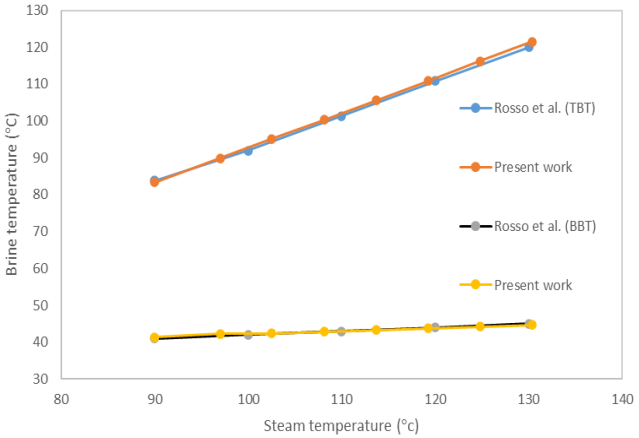

Figure 3: Effect of steam temperature on top brine temperature (TBT) and brine blowdown temperature (BBT)

The effect of steam temperature on the distillate production rate is presented in Figure 4. The results indicate that distillate production increases with increasing steam temperature, consistent with the thermodynamic behaviour of MSF systems. This increase is attributed to enhanced vapor generation at higher brine temperatures, leading to higher freshwater production.

The predicted trend follows the same general behaviour as the reference data; however, a noticeable deviation is observed, which increases with increasing steam temperature. At lower temperatures, the deviation remains relatively small (approximately 3–5%), while at higher steam temperatures it increases to about 6–8%, with the predicted distillate flow rate becoming progressively higher than the reference values.

This deviation can be attributed to differences in model formulation, particularly the section-wise representation adopted in the present model compared with the stage-by-stage approach of the reference model. These differences may lead to a slight accumulation of deviations in the estimation of vapor generation across the flashing stages, resulting in a

slight overprediction of distillate production at elevated temperatures.

The variation of the gain output ratio (GOR) with steam temperature is illustrated in Figure 5. The results show that GOR increases with increasing steam temperature, reflecting improved thermal utilization within the system. The predicted

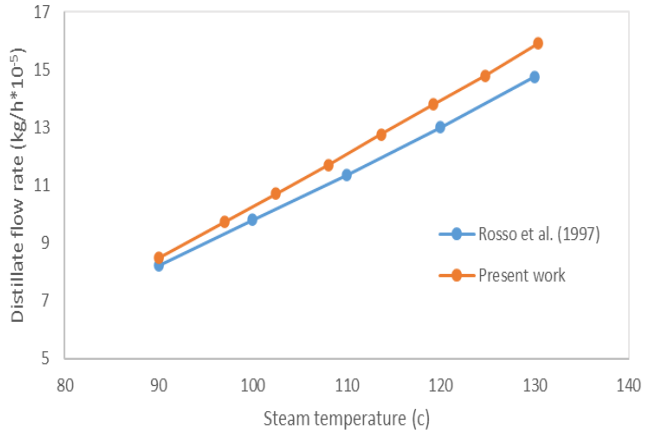

Figure 4: Effect of steam temperature on distillate production rate

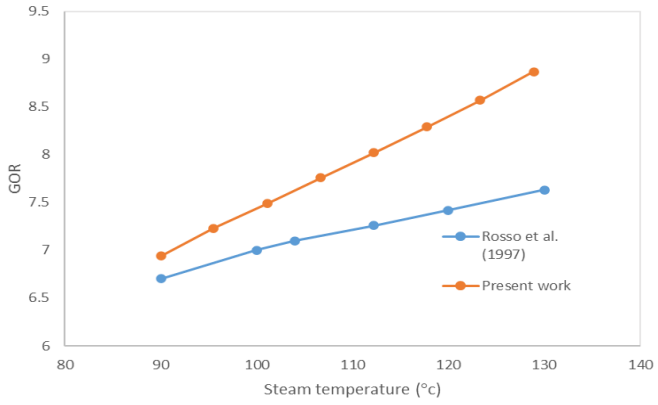

Figure 5: Effect of steam temperature on gain output ratio (GOR)

trend exhibits an approximately linear increase over the investigated temperature range, whereas the reference data shows a slightly lower rate of increase. Consequently, a noticeable deviation between the predicted and reference values develops, becoming more pronounced at higher steam temperatures.

Quantitatively, the deviation in GOR is relatively small at lower temperatures (about 5–7%) but increases significantly at higher steam temperatures, reaching approximately 13–16%. This behavior is consistent with the trends observed in Figure 4, where the present model slightly overpredicts the distillate production at elevated temperatures. Since GOR is directly proportional to the distillate flow rate, this leads to higher predicted GOR values.

It should also be noted that the larger deviations occur at relatively high steam temperatures, which correspond to operating conditions beyond the typical industrial range due to scaling limitations on the top brine temperature. Within the practical operating range, the agreement between the present model and the reference data remains satisfactory within the low-to-moderate steam temperature range.

Effect of sea water temperature

Figures 6–8 illustrate the effect of seawater inlet temperature on key performance parameters of the MSF-BR desalination system. The results show that variations in seawater temperature significantly influence system thermal conditions and performance. As the seawater temperature increases, the brine blowdown temperature (BBT) increases noticeably, while the top brine temperature (TBT) remains relatively less sensitive, reflecting the dominant role of the brine heater in controlling the upper temperature limit.

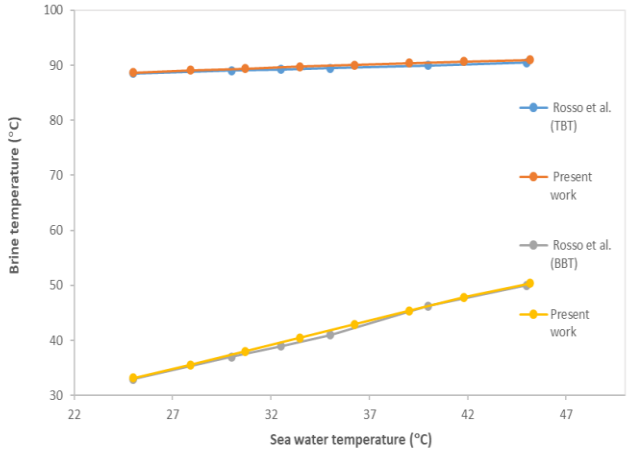

Figure 6: Effect of sea water temperature on top brine temperature (TBT) and brine blowdown temperature (BBT)

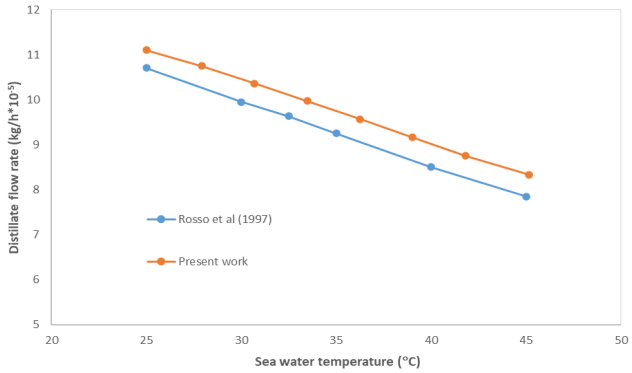

Figure 7: Effect of sea water temperature on distillate production rate.

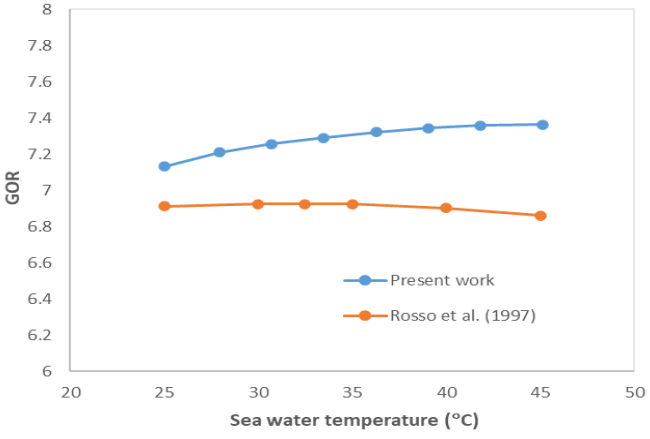

Figure 8: Effect of sea water temperature on gain output ratio (GOR)

The distillate production rate decreases with increasing seawater temperature, which is consistent with the reduced temperature driving force for heat transfer and flashing. The predicted values show good agreement with the reference data, with deviations generally within about 2–6% over the investigated temperature range. A slight overprediction is observed at higher seawater temperatures; however, the overall trend and slope are well captured by the model.

Similarly, the variation of the gain output ratio (GOR) with seawater temperature exhibits a weak and non-linear dependence. The predicted GOR values are consistently higher than the reference data, with deviations ranging approximately from 4% at lower temperatures to about 7% at higher temperatures. Despite this offset, the model successfully reproduces the overall trend and the relatively low sensitivity of GOR to seawater temperature.

Overall, the comparison confirms that the model accurately reproduces the sensitivity of MSF system performance to variations in seawater inlet temperature. The close agreement with the reference results, particularly in terms of trend and magnitude, indicates that the adopted formulation provides a reliable representation of the thermodynamic behavior of the system under varying intake conditions.

Conclusion

A steady-state mathematical model for brine-recycle multistage flash (MSF-BR) desalination plants has been developed and validated. The proposed formulation combines the computational efficiency of a section-wise approach with improved physical realism through the incorporation of temperature-dependent thermophysical properties. This improves the prediction of heat-transfer processes and temperature distributions while avoiding the complexity associated with fully stage-by-stage models.

The model was implemented in a FORTRAN environment and applied to a reference 5 MGD MSF-BR desalination plant. Validation against published data demonstrated good agreement for flow rates, temperatures, salinities, and heat-transfer coefficients. The model also reproduced the observed parametric trends associated with variations in steam and seawater temperatures. Although a slight overprediction of distillate production and gain output ratio (GOR) was observed at elevated steam temperatures, the agreement remained satisfactory within the practical operating range of MSF systems.

The results confirm that the proposed formulation reliably captures the coupled heat- and mass-transfer behavior of MSF-BR desalination systems under steady-state conditions. The adopted section-wise representation significantly reduces computational effort while preserving the dominant thermodynamic characteristics of the process. In addition, the incorporation of variable thermophysical properties improves prediction accuracy compared with conventional simplified models that assume constant properties throughout the plant.

Owing to its balance between predictive capability and computational simplicity, the proposed model provides a practical tool for simulation, performance evaluation, parametric analysis, and preliminary optimization of existing and future MSF desalination plants.

Despite the satisfactory agreement obtained with published reference data, further validation using industrial plant measurements would be beneficial, particularly under high-temperature operating conditions where publicly available experimental data remain limited. Such validation would support further assessment and refinement of the model for practical large-scale desalination applications.

Nomenclature
Roman Symbols

Symbol	Description	Units
A	Heat-transfer area	m²
A_H	Heat-transfer area of the brine heater	m²
A_R	Heat-transfer area per stage in the recovery section	m²
A_J	Heat-transfer area per stage in the rejection section	m²
B	Brine flow rate	kg·h⁻¹
B_1, B_2, B_D	Brine flow rates at different plant locations	kg·h⁻¹
C_B	Brine salinity	wt.%
$C_{B_0}, C_{B_1}, C_{B_2}$	Brine salinity at specified sections	wt.%
C_F	Feed seawater concentration, mass fraction	wt.%
D	Distillate flow rate	kg·h⁻¹
D_1, D_2	Distillate production in recovery and rejection sections	kg·h⁻¹
F	Make-up seawater flow rate	kg·h⁻¹
GOR	Gain output ratio	–
L	Tube length	m
N	Number of stages	–
N_R	Number of stages in the recovery section	
N_J	Number of stages in the rejection section	
R	Recycle brine flow rate	kg·h⁻¹
S	Mean specific heat capacity	kcal·kg⁻¹·K⁻¹
S_B	Mean specific heat capacity of brine	kcal·kg⁻¹·K⁻¹
S_D	Mean specific heat capacity of distillate	kcal·kg⁻¹·K⁻¹
S_F	Mean specific heat capacity of make-up seawater	kcal·kg⁻¹·K⁻¹
S_J	Mean specific heat capacity of cooling brine (rejection section)	kcal·kg⁻¹·K⁻¹
S_R	Mean specific heat capacity of cooling brine (recovery section)	kcal·kg⁻¹·K⁻¹
S_{RY}	Mean specific heat capacity of recycle brine	kcal·kg⁻¹·K⁻¹
S_W	Mean specific heat capacity of cooling brine at inlet recovery section	kcal·kg⁻¹·K⁻¹
T	Temperature	°C
T_B	Brine temperature	°C
T_{B_0}	Top brine temperature (TBT)	°C
T_{B_1}, T_{B_2}	Brine temperatures leaving recovery and rejection sections	°C
T_D	Distillate temperature	°C
T_{D_1}, T_{D_2}	Distillate temperatures leaving recovery and rejection sections	°C
T_F	Cooling seawater temperature	°C
$T_{F_1}, T_{F_2}, T_{F_3}, T_{F_4}$	Cooling-brine temperatures at section inlets and outlets	°C
T_S	Saturated steam temperature supplied to the brine heater	°C
T^*	Reference temperature for energy balance	°C
U	Overall heat-transfer coefficient	kcal·h⁻¹·m⁻²·°C⁻¹
U_R	Heat-transfer coefficient in recovery section	kcal·h⁻¹·m⁻²·°C⁻¹

Symbol	Description	Units
U_J	Heat-transfer coefficient in rejection section	kcal·h⁻¹·m⁻²·°C⁻¹
U_H	Heat-transfer coefficient in brine heater	kcal·h⁻¹·m⁻²·°C⁻¹
W	Cooling brine mass flow rate (recovery section)	kg·h⁻¹
W_T	Cooling seawater flow rate (rejection section)	kg·h⁻¹
W_S	Steam flow rate to the brine heater	kg·h⁻¹

Greek symbols

Symbol	Description	Units
a_{i_R}, a_{i_J}, a_M	Intermediate coefficients	
b_{i_R}, b_{i_J}, b_M	Intermediate coefficients	
C_{i_R}, C_{i_J}, C_{i_H}, C_{i_M}	Linearization coefficients	
λ	Latent heat of vaporization of water	kcal·kg⁻¹
α	Heat-transfer effectiveness parameterType equation here.	-
Δ	Temperature loss across the demister	°C
BPE	Boiling point elevation	°C
NEA	Non-equilibrium allowance	°C

Subscripts

0	Top brine or inlet condition
1, 2	Section or stage index
B	Brine
D	Distillate
F	Feed seawater
H	Brine heater
R	Recovery section
J	Rejection section
sat	Saturation condition

Author Contributions: **Abduljawad**: Conceptualization, methodology, simulation, writing original manuscript. The author has read and approved the final version of the manuscript for publication.

Conflict of interest: "The author declares that there are no conflicts of interest."

Funding: "This research received no external funding."

Data Availability Statement: "The data supporting the findings of this study are available from the corresponding author upon reasonable request."

References

[1] J. Eke, A. Yusuf, A. Giwa, and A. Sodiq. "The global status of desalination: An assessment of current desalination technologies, plants and capacity." *Desalination*, vol. 495, pp. 114633, 2020. https://doi.org/10.1016/j.desal.2020.114633

[2] D. Curto, V. Franzitta, and A. Guercio. "A Review of the Water Desalination Technologies." Applied Sciences, vol. 11, no. 2, p. 670, 2021. https://doi.org/10.3390/app11020670

[3] A. Fadiel, et al. "Desalination in Libya (2000-2025): A Strategic Review of Technological Evolution," Institutional Challenges and Pathways toward Water Security, pp. 1-23, 2025: http://dx.doi.org/10.2139/ssrn.5602070

[4] M Elnaggar, et al. "Design of a solar thermal powered system for electricity generation and water desalination." In 8th International Engineering Conference on Renewable Energy & Sustainability *(ieCRES)*, 08-09 May 2023, Gaza, Palestine. https://doi.org/10.1109/ieCRES57315.2023.10209513

[5] H. El-Khozondar, et al. "Linear Fresnel collector (LFC) for enhancing solar water desalination process." In *8th International Engineering Conference on Renewable Energy & Sustainability (ieCRES)*, 08-09 May 2023, Gaza, Palestine. https://doi.org/ 10.1109/ieCRES57315.2023.10209535

[6] A. Coleman. "Optimization of a single effect, multi-stage flash distillation desalination system." *Desalination*, vol. 9, pp. 315–331, 1971. https://doi.org/10.1016/0011-9164(71)80002-4

[7] M. Soliman. "A mathematical model for MSF multi-stage flash desalination plants." *Journal of Engineering Sciences*, vol. 7, no. 2, pp. 143–150, 1981.

[8] M. Darwish. "Thermal analysis of multi-stage flash desalting system." *Desalination*, vol. 85, pp. 59–79, 1991. https://doi.org/10.1016/0011-9164(91)85147-M

[9] H. El-Dessouky, I. Alatiqi, and H. Ettouney. "Process synthesis: The multi-stage flash desalination system." *Desalination*, vol. 115, pp. 155–179, 1998. https://doi.org/10.1016/S0011-9164(98)00035-6

[10] A. Helal, M. Medani, M. Soliman, and J. Flower. "Tridiagonal matrix model for multistage flash desalination plants." *Computers & Chemical Engineering*, vol. 10, no. 4, pp. 327–342, 1986. https://doi.org/10.1016/0098-1354(86)87003-X

[11] A. Hussain, A. Hassan, D. Al-Gobaisi, A. Al-Radif, A. Woldai, and C. Sommariva. "Modeling, simulation, optimization and control of multistage flash (MSF) desalination plants—Part 2: Modeling and simulation." *Desalination*, vol. 92, pp. 21–41, 1993. https://doi.org/10.1016/0011-9164(93)80074-W

[12] N. Aly, and A. El-Fiqi. "Thermal performance of seawater desalination systems." *Desalination*, vol. 158, pp. 127–142, 2003. https://doi.org/10.1016/S0011-9164(03)00443-0

[13] H. El-Dessouky, H. Shaban, and H. Al-Ramadan. "Steady state analysis of multi-stage flash desalination process." *Desalination*, vol. 103, pp. 271–280, 1995. https://doi.org/10.1016/0011-9164(95)00080-1

[14] M. Rosso, A. Beltramini, M. Mazzotti, and M. Morbidelli. "Modelling of multistage flash desalination plants." *Desalination*, vol. 108, pp. 365–374, 1997. https://doi.org/10.1016/S0011-9164(97)00046-5

[15] F. Alasfour and H. Abdulrahim. "Rigorous steady-state modeling of MSF-BR desalination system." *Desalination and Water Treatment*, vol. 1, pp. 259–276, 2009. https://doi.org/10.5004/dwt.2009.300

[16] M. Abduljawad, and U. Ezzeghni. "Optimization of Tajoura MSF desalination plant." *Desalination*, vol. 254, pp. 23–28, 2010. https://doi.org/10.1016/j.desal.2009.12.019

[17] W. Abujazyah. "Modelling and simulation of multistage flash desalination plants/" *Libyan Journal for Engineering Research*, vol. 1, no. 2, pp. 43–47, Sep. 2017.

[18] M. Hassanean, A. Nafey, R. El-Maghraby, and F. Ayyad. "Simulation of multi-stage flash with brine circulating desalination plant." *Journal of Petroleum and Mining Engineering*, vol. 21, no. 1, pp. 34–42, 2019. https://doi.org/10.21608/jpme.2020.73173

[19] M.S. Tanvir, I.M. Mujtaba, (2006). Modelling and simulation of MSF desalination process using gPROMS and neural-network based physical property correlation, Computer Aided Process Engineering 21, 315–320.

[20] E. Hawaidi, and I. Mujtaba. "Sensitivity of brine heater fouling on optimization of operation parameters of MSF desalination process using gPROMS." in: Proceedings of 20th European Symposium on Computer Aided Chemical Engineering, Naples, pp. 1787–1792, 2010.

[21] H. Al-Fulaij. "Dynamic modeling of multi stage flash (MSF) desalination plant." PhD Thesis, University College London, 2011.

Appendix A: Thermophysical Property Correlations

Eq. (A.1). Enthalpy of saturated water

$$h_D = \left(-31.92 + 1.0011833T_D - 3.083326 \times 10^{-5}{T_D}^2 + 4.666663 \times 10^{-8}{T_D}^3 + 3.333334 \times 10^{-10}{T_D}^4\right) \times 1.8$$

h_D= specific enthalpy of saturated water (kcal/kg)
T_D = temperature (°F)
The factor 1.8 converts the correlation to kcal/kg.

Eq. (A.2). Superheated steam enthalpy

$$h_V = (596.912 + 0.46694T - 4.60256 \times 10^{-4}T^2) \times 1.8$$

h_V = specific enthalpy of superheated steam (kcal/kg)
T = temperature (°C)

Eq. (A.3). Latent heat of vaporization of wate

$$\lambda = h_V - h_D$$

λ = latent heat of vaporization (kcal·kg⁻¹)

Eq. (A.4). Specific heat capacity of pure water

$$S_D = 1.0011833 - 6.1666652 \times 10^{-5}\ T + 1.3999989 \times 10^{-7}\ T^2 + 1.3333336 \times 10^{-9}\ T^3$$

S_D= specific heat of water (kcal/kg·°C)
T = boiling temperature of water (°F)

Eq. (A.1). Heat capacity of brine

$$S_b = [1 - \mathrm{CB}(0.011311 - 1.146 \times 10^{-5}\ T_b)]S_D$$

S_b = specific heat of brine (kcal·kg⁻¹·°C⁻¹)
S_D = specific heat of water (kcal·kg⁻¹·°C⁻¹)
T_b = brine temperature (°F)
CB = salt concentration (wt%)

$$CB(wt\%) = C_b(massfraction) \times 100$$

Eq. (A.1). Density of brine

$$\rho = 16.01846\ (62.707172 + 49.364088\ \mathrm{C_b} - 0.43955304 \times 10^{-2}\ \mathrm{T_b} - 0.032554667\ \mathrm{C_b T_b} - 0.46076921 \times 10^{-4}\ {\mathrm{T_b}}^2 + 0.63240299 \times 10^{-4}\ \mathrm{C_b}\ {\mathrm{T_b}}^2)$$

ρ = brine density (kg·m⁻³)
$\mathrm{T_b}$ = brine temperature (°F)
$\mathrm{C_b}$ = salt concentration (mass fraction)

Eq. (A.7). Boiling point elevation (BPE)

$$BPE = (C\ T^2\ /\ (266919.6 - 379.669\ T + 0.334169\ T^2))\ [565.757\ /\ T - 9.81559 + 1.54739\ ln(T) - C\ (337.178\ /\ T - 6.41981 + 0.922753\ ln(T)) + C^2\ (32.681\ /\ T - 0.55368 + 0.079022\ ln(T))]$$

T = brine temperature (K)
*C = 19.819 * Cb / (1 - Cb)*
Cb = salt concentration (mass fraction)

Eq. (A.8). Non-equilibrium allowance (NEA)

$$NEA = \left[195.556\ {H_j}^{1.1}\ (\omega_j \times 10^{-3})^{0.5}\right] / \left[(\Delta T_{B_j})^{0.25}\ {T_D}_j{}^{2.5}\right]$$

H_j = height of brine pool in stage j (in)
$\Delta T_{B_j} = T_{B_j} - T_{B_{j-1}}$ (°F)
$\omega_j = W/w_j$ (lb/h/ft) , mass flow rate per unit stage width ($lb \cdot h^{-1} \cdot ft^{-1}$)
w_j = width of stage (for cross tube design only) (ft),
${T_D}_j$=saturation temperature corresponding to the prevailing pressure in the stage (°F).

Eq. (A.9). Temperature loss across the demister

$$\Delta = exp(1.885 - 0.02063\ T_D)/1.8$$

Δ = temperature loss (°C)
TD = condensing vapor temperature (°F)

Eq. (A.10). Overall heat transfer coefficient

$$z = 0.1024768 \times 10^{-2} - 0.7473939 \times 10^{-5}\ T_D + 0.999077 \times 10^{-7}\ {T_D}^2 - 0.430046 \times 10^{-9}\ {T_D}^3 + 0.6206744 \times 10^{-12}\ {T_D}^4$$

$$y = \left((vD_i)^{0.2} / ((160 + 1.92\ T_{HE})v)\right)$$

$$U = 4.8857\ /\ (y + z + 4.8857\ f)$$

U = overall heat transfer coefficient ($kcal \cdot h^{-1} \cdot m^{-2} \cdot °C^{-1}$)
v = linear velocity of brine stream (ft/s)
D_i= internal tube diameter (in)
T_{HE} = brine temperature at exit of heat exchanger (°F)
f = fouling fac